Progress In Electromagnetics Research M, Vol. 109, 1–12, 2022

Towards Localization and Classification of Birds and Bats in Windparks Using Multiple FMCW-Radars at Ka-Band

Ashkan Taremi Zadeh*, Murat Diyap, Jochen Moll, and Viktor Krozer

Abstract—Birds and bats are at risk when they are flying near wind turbines (WT). Hence, a protection of bats and birds is postulated to reduce their mortality, e.g., due to collisions with the rotor-blades. The use of radar technology for monitoring wind energy installations is becoming increasingly attractive for WT operators, as it offers many advantages over other sensor systems. Timely localization and classification of the approaching animal species is very crucial about the reaction measures for collision avoidance. In this work, a localization, classification, and flight path prediction technique has been developed and tested based on simulated radar signals. This allowed us to classify three different birds and one bat species with an accuracy of 90.18%. For accurate localization and target tracking, five frequency modulated continuous wave (FMCW) radars operating in Ka-Band were placed on the tower of the WT for 360° monitoring of the WT.

1. INTRODUCTION

The continuous increase of wind energy worldwide constitutes a significant threat to birds and bats [1, 2]. Every year, thousands of birds and bats die either through direct collision with wind turbines (WT) or, especially in the case of bats, through barotrauma effects [3, 4]. In order to protect these endangered species, governments in many countries, including Germany, have adopted various measures to reduce the mortality of these species. In Germany, many WTs are currently affected by shutdown algorithms to avoid collision of bats with turbines during seasons and times with high bat activity [5]. These algorithms are now the most common minimization measure to reduce operational bat kills at WTs in Germany. In areas with many protected bird species like red kites, there are even building restrictions. These minimization measures are an integral part of the planning of WT. Although these laws protect the animals from extinction, they are detrimental to achieving climate goals and the profitability of WTs.

For years, there has been a lot of research to develop systems with the goal of minimizing shutdown times and also obtaining building permits even for areas with high bird activity. This can be achieved, for example, by recognizing the approaching bird or bat in time and reacting accordingly. So far, different methods have been used to detect and classify birds and bats. Many WT operators use camera-based systems to detect and classify birds using camera images and neural networks [6–9]. Here, high-resolution cameras are used to detect the animals at large distances. The performance of these systems is however strongly limited by weather conditions and good light conditions. Even with optimal conditions no good classification can be achieved in large distances, because only a few pixels are visible on the images, which make the classification difficult.

Therefore, other methods like radars are more suitable, because they are less dependent on weather or light conditions and are able to detect moving objects even at great distances. Hence, radar systems have been considered as a promising approach in recent years. In [10–12], different methods

Received 5 November 2021, Accepted 20 January 2022, Scheduled 4 March 2022
* Corresponding author: Ashkan Taremi Zadeh (ashkan.taremi@gmail.com).
The authors are with the Department of Physics, Physikalisches Institut, Goethe-University Frankfurt, Germany.

were proposed to classify birds by micro Doppler signatures, which are generated by the wing beat. Mostly convolutional Neural Network is used for the classification. In addition, other signal processing techniques exist such as continuous wavelet transform in which the wing beat patterns are used for the classification [13]. So far, there is no reliable method of species detection by radar. A method with which it is possible to distinguish different species would be a great advance for collision avoidance.

In this work, we have developed a new method to classify different bird and bat species by analyzing the back scattered energy coming from the wing beat of the flying animals. In addition, localization and classification algorithms were developed based on numerical data which we can determine the location of the birds using multi-radar technology and predict the flight path using predictive analysis. The timely localization and classification of the animals approaching the WT could can lead to an adaptive WT control strategy so that currently implemented shutdown algorithms leading to revenue losses can be overcome.

2. SIMULATION ENVIRONMENT

In order to find a suitable localization and classification method, the simulation environment had to be implemented realistically. The radar system operates in frequency-modulated continuous wave (FMCW) mode in the frequency band from 33.4 to 34.15 GHz. The output power of the radar sensor is about 30 dBm and an antenna gain of 20.28 dBi. In the simulation, a WT of type Vestas V100-2.0 MW with a nacelle height of 80 meters and a rotor blade length of 49 m is located in the center of the coordinate system in $P_{WT} = [x\ y\ z] = [0\ 0\ 0]$. In order to find the optimal position of the radar systems for all-round coverage of the WT, we carried out a numerical study in [14]. Through this work we have found that we need at least five radar systems for optimal coverage around the WT, which should be attached to the WT tower at a height of 15 m and an elevation angle of 75°. Figure 1 shows the simulation environment. In order to have enough time for a suitable reaction for approaching animals, we defined a danger zone with a radius of 400 m. If an object approaches with a speed of 10 $\frac{\text{m}}{\text{s}}$, the WT has 40 s to shut down.

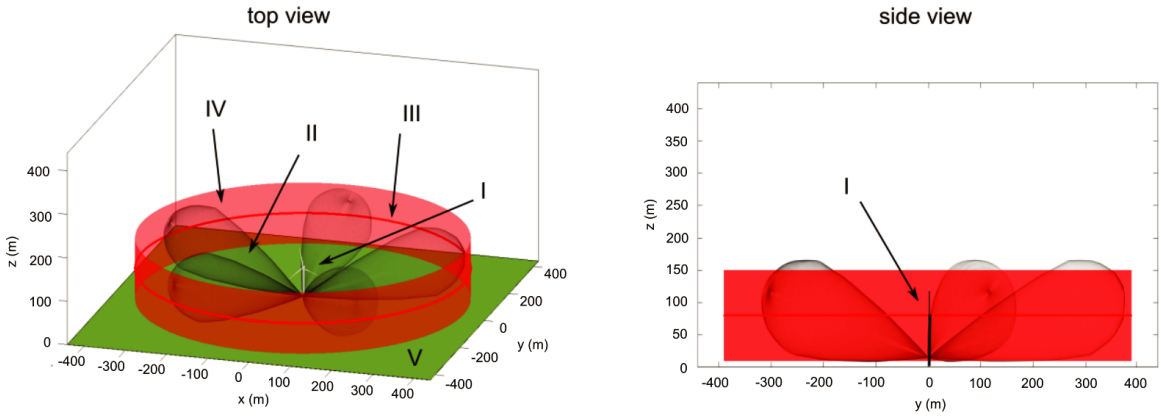

Figure 1. Simulation environment with WT model. In this figure the WT is marked with I, antenna diagram with II, the reference height of the nacelle with III, the border of the danger zone with IV and the ground with V [14].

The simulation is based on the weighting of the radar target by the antenna diagram. The antenna diagram, shown in Figure 4, consists of the polar angle θ, the azimuthal angle ϕ and amplitude A in spherical coordinates. The radar signal is compared and weighted according to the position $P_{Target} = (\theta_{target}, \phi_{target}, r_{target})$ of the radar target with the antenna diagram. More information about this antenna can be found in [15].

The simulation of the radar signal is shown schematically in Figure 2, which is described in more detail in Section 2.1.

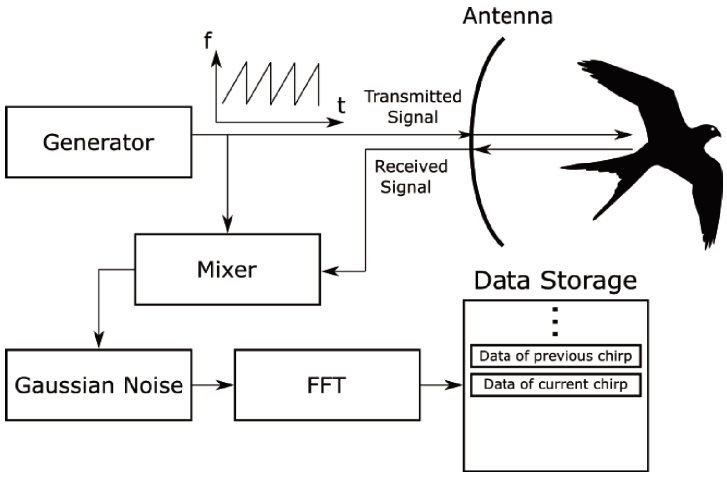

Figure 2. Schematic representation of the signal model used in the simulation.

2.1. Transmitted Signal Model

The transmitted signal can be expressed by a sinusoidal function with a frequency f. The frequency of the simulated FMCW radar increases linearly with a slope α:

$$f = f_c + \alpha t \tag{1}$$

$$\alpha = B/T \tag{2}$$

where $f_c = 33.775\,\text{GHz}$ is the carrier-frequency; T is the duration of a chirp; and B is the bandwidth of a chirp. B and T are set to 750 MHz and 2.56 ms, respectively. The phase of the transmitted signal is given by the integral of the frequency with respect to time multiplied by 2π. The transmitted signal can hence be expressed as [16]:

$$s_t(t) = \cos\left(2\pi\left(f_c t + \frac{1}{2}\alpha t^2\right)\right) \tag{3}$$

2.2. Received and Mixed Signal Models

The power of the backscattered radiation S_r from an object at a distance R and an incident power density S_i is proportional to its radar cross section (RCS). The RCS has following definition [17]:

$$\sigma = \lim_{R\to\infty} 4\pi R^2 \frac{S_r}{S_i} \tag{4}$$

The power P_r of the signal which is backscattered from an object with a RCS σ at a distance R is given by the radar equation [18]:

$$P_r = \frac{P_t G^2 \sigma \lambda^2}{(4\pi)^3 R^4} \tag{5}$$

where P_t, G, and λ are the transmitted power, the gain factor, and the wavelength of the transmitted radiation, respectively. The amplitude A of the backscattered signal is proportional to the square root of P_r. Since the calibration factor is unknown, in the simulation it is assumed that $A = \sqrt{P_r}$.

The backscattered signal from an object is delayed relative to the transmitted signal by a time τ. This leads to the following expression for the backscattered signal [16]:

$$s_r(t) = A \cdot \cos\left(2\pi(f_c(t-\tau) + \frac{1}{2}\alpha\left(t-\tau\right)^2)\right) \tag{6}$$

Assuming that the object is initially at a distance R from the radar and has a constant radial velocity v, the time delay is $\tau = 2(R + vt)/c$. For an ideal receiver the intermediate frequency signal (IF) is

obtained by multiplying the transmitted signal with the received signal, which leads to a high frequency and a low frequency term. The high frequency term is filtered out, resulting in [16]:

$$s_{IF}(t) = A{\cdot}\cos\left(2\pi\left(\alpha t\tau + f_c\tau - \frac{1}{2}\alpha\tau^2\right)\right) = A{\cdot}\cos(4\pi(\alpha t(R{+}vt)/c{+}f_c(R{+}vt)/c{-}\alpha(R{+}vt)^2/c^2)) \quad (7)$$

In this equation the terms of order $1/c^2$ and t^2 are negligibly small compared to the others. This leads to the following approximated expression for $s_{IF}(t)$:

$$s_{IF}(t) \approx A \cdot \cos\left(2\pi\left(\frac{2\alpha Rt + 2f_c vt + 2f_c R}{c}\right)\right) \quad (8)$$

The first summand in the cosine function describes the frequency shift due to the time-delay between the transmitted and received signals, while the second term represents the Doppler frequency shift. The third term represents a constant phase shift, which is related to the initial distance between the radar and the object.

2.3. Noise Model

In order to make the simulation more realistic, the received signal is superimposed with thermal noise, which can be described by a Gaussian function [19]. In the simulation the thermal noise is modeled by generating a random voltage according to a Gaussian distribution for each sampling point. The average noise power is given by the variance of this Gaussian distribution, which increases linearly with the temperature of the receiver and the bandwidth of the signal [20]. The simulation can be done for different signal to noise ratios (SNRs). For these simulations, a signal to noise ratio of 1 dB was assumed. Considering the noise level present in the received signal, the radar equation of a monostatic radar can be extended to obtain the expression of the radar SNR as follows [21]:

$$SNR = \frac{P_T G^2 \sigma \lambda^2}{(4\pi)^3 R^4 k T B F_n} \quad (9)$$

with the antenna gain G, transmit power P_T, target distance R, temperature T, bandwidth B, Boltzmann constant k, and noise figure F_n.

2.4. Bird Model

The birds are modelled by 5 dynamically connected points as shown in Figure 3. The central point represents the body, while the other four points represent the tips of the left/right upper wing and forewing. The total received signal is obtained by superposition of the signals received from each point. The wing-points move in the plane, which is perpendicular to the flight-direction of the bird. The angle between the xy-plane and the vector of the upper wing is represented by β, while γ represents the angle between the xy-plane and the vector of the forewing as shown in Figure 3. Both angles vary sinusoidally with the wingbeat frequency f. A full wingbeat period consists of an up- and a downstroke. During the downstroke the wings are extended in order to maximize the lifting force, while the bird folds its wings during upstroke in order to minimize the counterproductive downing force [22]. In Figure 3 the picture at $t = 0$ shows the beginning of a downstroke, when the angle $\beta(t)$ is at a maximum. At that time the bird unfolds its wings by increasing the angle $\gamma(t)$ in order to maximize the lifting force during the following downstroke. In the simulation this is taken into account by delaying $\gamma(t)$ by $\pi/4$ with respect to $\beta(t)$. The mathematical implementation is as follows:

$$\beta(t) = 60^\circ \cdot \cos(\omega t) \quad (10)$$

$$\gamma(t) = 60^\circ \cdot \cos(\omega t - \pi/4) - 10^\circ \quad (11)$$

where ω is the angular wing beat frequency of the bird. Figure 3 visualizes the motion of the wings by showing an equidistant time series of wing positions during a full wing beat period.

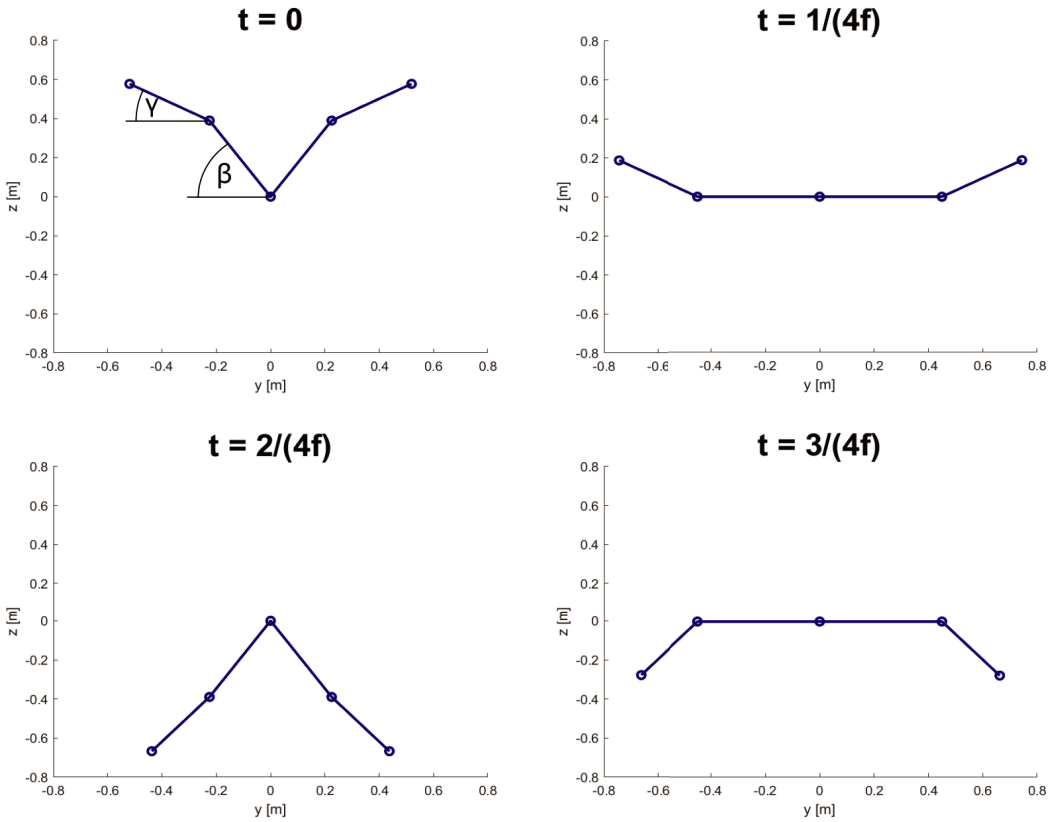

Figure 3. Equidistant time series of a full wingbeat period.

2.5. Dynamic RCS Model of the Wings

The radar cross section of birds is of the order of $0.01\,\mathrm{m}^2$ [23]. While the RCS of the body is nearly constant during a wingbeat period, the RCS of the wings varies with their positions [24]. Since information about the distribution of the RCS between the body and the wings for the analyzed bird species is not available in the literature, we assume in the simulation that the RCS of the body is one half of the total RCS σ, while the RCS of each wing point equals $\frac{\sigma}{8}$ if the radar beam hits the corresponding wing plane vertically. The value of σ depends on the simulated bird species.

The RCS for each of the four wing points is assumed to be proportional to the power of the radiation hitting the surface of the corresponding wing plane. The proportionality factor is given by the cosine of the incident angle θ of the radar beam on a wing-plane. It is assumed that the wing plane of each upper wing is spanned by the vector of the flight direction of the bird and the vector connecting the body with the tip of each upper wing, while the wing plane of each forewing is spanned by the vector of flight direction and the vector connecting each tip of a upper wing with the tip of the corresponding forewing. The RCS of the wing points σ_i is calculated as follows:

$$\sigma_i = \frac{\sigma}{8} \cdot \cos(\theta_i) \tag{12}$$

where i is an index representing the four wing points.

2.6. Classification

The radar signals generated by different bird species are analyzed through numerical simulations. Different features such as wing beat frequency, RCS, and radial flight speed can be extracted from the IF-signal. The wing beat frequency can be extracted by calculating the backscattered energy of the radar signals generated by the motion of the wings relative to the body. One goal of this analysis is to predict the correct bird species based on these extracted features (see Section 3.2). The classification

is done by a machine-learning algorithm, which needs training data as input. We have performed 1140 simulations in which 75% of the data were used for the training and 25% for the validation. The training data are generated by simulating the flight of a bird for a certain amount of time and then extracting the relevant features from the computed IF-signal. This is done for different bird species at different starting positions, flight speeds and flight directions.

It should be comprehensible, in which way the algorithm uses the features to makes its predictions. This is possible for a Decision Tree or a Support Vector Machine (SVM) by visualising the tree or the decision regions respectively, and since the algorithms later have to learn and analyze the data in real time, it is also important that the algorithms are fast and also have a high degree of accuracy. Decision Trees have been shown to be suitable when classifying drones and birds. In [25], the authors used a Decision Tree classifier and could already show the effectiveness of the Decision Trees at filtering out non-drone targets like birds.

2.7. Simulations

Figure 4 shows different simulations performed for this study. For this purpose, we simulated all possible scenarios that can occur during a bird flight. For this we simulated the straight flights in different angles (5° steps between 0° and 90°), the flights in different heights (5 m steps between 10 m and 120 m) and the curved flights by randomly chosen flight radius (between 10 m and 50 m). All these simulations were performed for the distances 50 m, 100 m, 150 m, 200 m, 300 m, and 400 m.

Four different animals have been considered, i.e., a red kite (Milvus milvus), a pigeon (Columbidae), a songbird (Alauda arvensis), and a bat (Eptesicus serotinus). The red kite has a RCS of 0.01 m^2 with a mean wingspan of 1.6 m and a wingbeat frequency of 2.8 Hz (SD ±0.5) [26]; the pigeon has a RCS

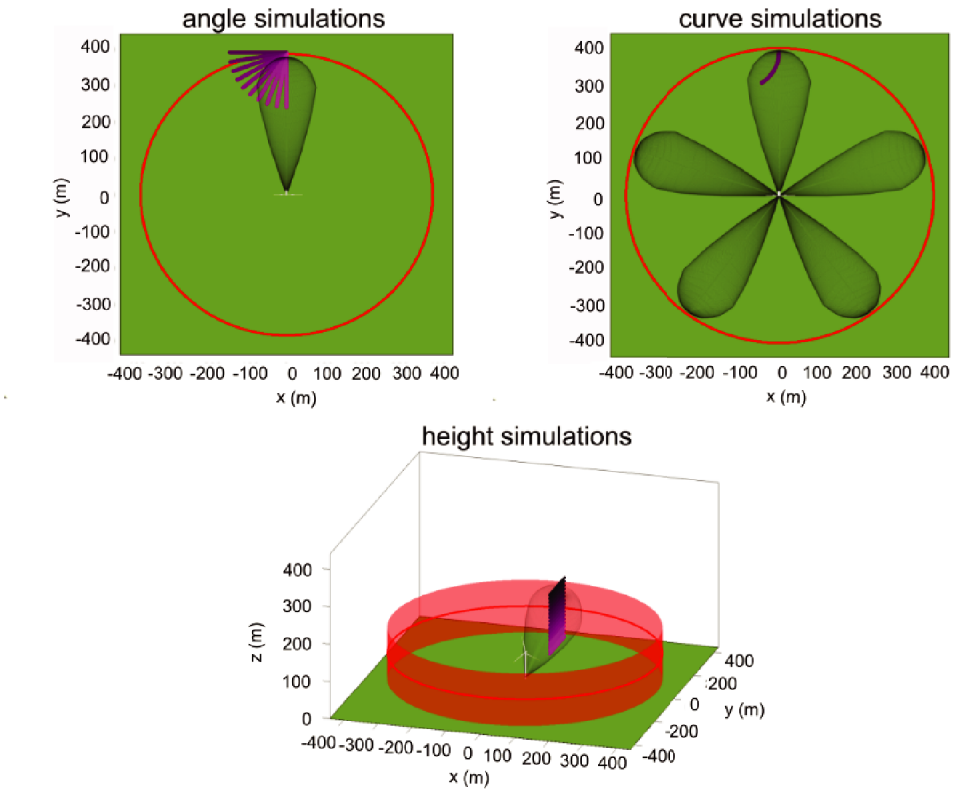

Figure 4. In angle simulations the flight trajectories of a bird in different angels towards and away from the WT is depicted. Through curve simulations we have simulated the scenario in which the bird does not perform a straight line flight, but flies a curve. In height simulations the flight trajectories of a bird in different heights towards the WT is simulated.

of 0.01 m^2 with a mean wingspan of 0.68 m and a wingbeat frequency of 5.5 Hz (SD ±0.2) [27]; the songbird has a RCS of 0.0005 m^2 with a mean wingspan of 0.4 m and a wingbeat frequency of 9.8 Hz (SD ±0.8) [26]; and the bat has a RCS of 0.00021 m^2 with a mean wingspan of 0.32 m and a wingbeat frequency of 7.5 Hz (SD ±0.63) [28, 29]. In addition to the wing beat, we also simulated gliding flights for red kite ($f_{wingbeat} = 0$ Hz) by having the bird glide through the air.

3. RESULTS

3.1. Localization

By using multiple radar systems looking in different directions, localization of the object can be achieved in real time by amplitude analysis. Therefore, we have developed algorithms that estimate the position of the object by analyzing the amplitude of all radar signals. For example, if the threshold is crossed only for radar 1 but not for other radars, the object is located in front of radar 1. If the threshold is crossed for radar 1 and radar 2, the object must be located between these two radars. By this information and the distance information which is available by FMCW radars, a localization can be achieved. Figure 5 visualizes how the algorithm works. Since the FMCW radar only provides distance information, accurate localization of the object becomes infeasible. For this reason, the algorithm calculates a possible position, which is marked in red in Figure 5. Each point on this red sphere surface has the same distance to the radar.

For collision avoidance measures, it is not enough to know where the object is, but also whether the object is approaching or moving away. In order to predict the position of the bird in the next seconds, we have extended the localization algorithms to predict the position of the object in the future. For this,

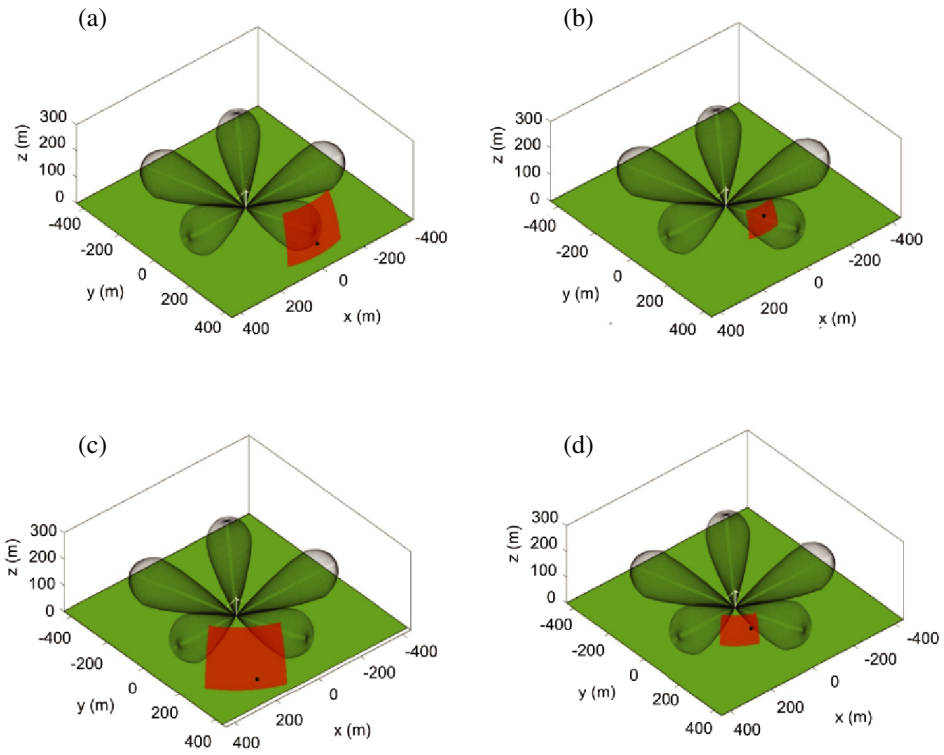

Figure 5. Visualization of the localization algorithm. The black dot represents the approaching object and and the red area is the area calculated by the algorithm where the object may be located. In (a) the bird is located in a distance of 400 m in front of the first radar, in (b) the bird is located in a distance of 200 m in front of the first radar, in (c) the bird is located in 400 m between the first and the second radar and in (d) the bird is located between the first and second radar in a distance of 200 m.

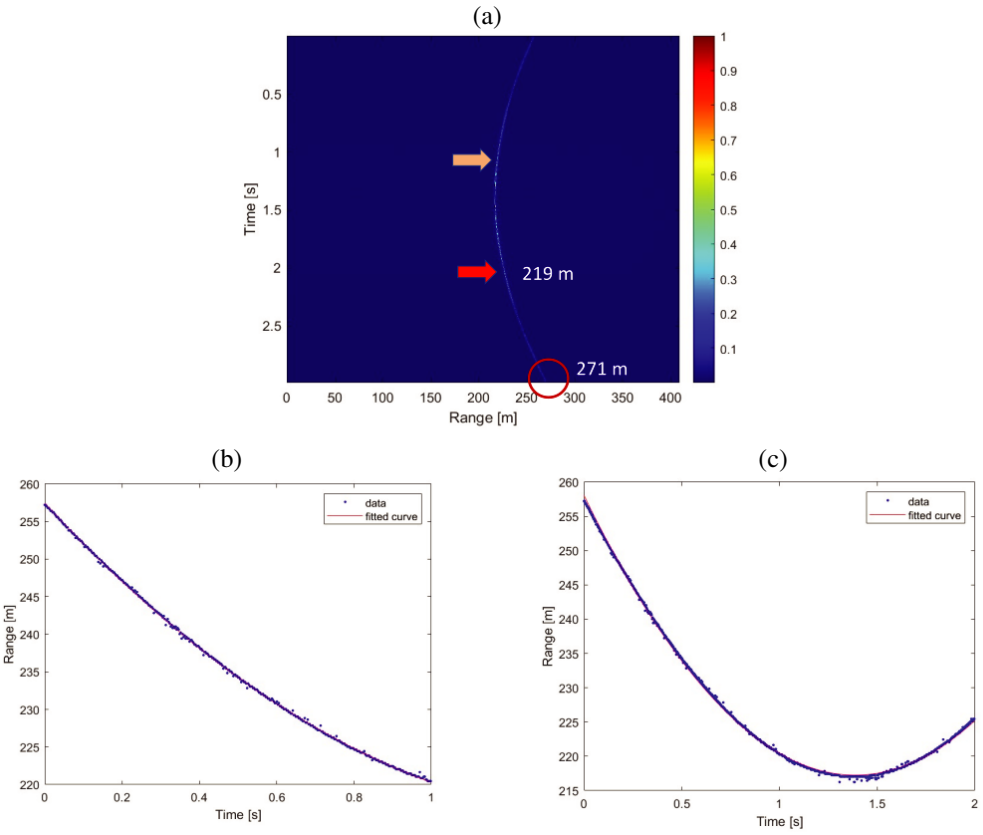

Figure 6. (a) Shows the radargram of a simulation in which the bird approaches the WT at the beginning and then moves away. (b) Shows the first analysis moment, marked with an yellow arrow in Figure (a). (c) Shows the second moment of analysis, marked with an red arrow in Figure (a). The values depicted on the radargram are the results of the range estimation by the polynomial regression algorithm.

we used a polynomial regression to predict the position in the next second. Polynomial Regression is a form of regression analysis in which the relationships between the independent variables and dependent variables are modeled in the nth degree polynomial [30]:

$$y_i = \alpha_0 + \alpha_1 x_i + \alpha_2 x_i^2 + \ldots + \alpha_m x_i^m + \epsilon_i \ (i = 1, 2, \ldots, n) \tag{13}$$

where ϵ_i is an unobserved random error with mean zero conditioned on a scalar variable x_i and the unknown parameters α_m. In Figure 6, the radargram of a simulation is depicted, in which at the beginning the bird is approaching the WT and then moves away from the WT. The yellow arrow shows the moment of the first analysis. After one second of data acquisition, we run the first analysis with polynomial regression (Figure 6(b)), and after another second, which is marked with a red arrow, we make another analysis (Figure 6(c)). With this method we repeat the analysis every second and can estimate the position of the object for the next second. The results of the regression are also depicted on the radargram. In the first analysis, a distance of 219 m is estimated and in the second analysis a distance of 271 m. By this method, in addition to the position information we get from multi-radar, we know if the object is approaching or moving away from us.

3.2. Classification

For the classification of the birds, finding suitable features is very crucial. Therefore, the size of the birds and wing beat frequency are extremely important. To extract the wing beat frequency of birds, first we calculate the energy of the Fourier transformed signal from each row of the radargram R_{ij} and

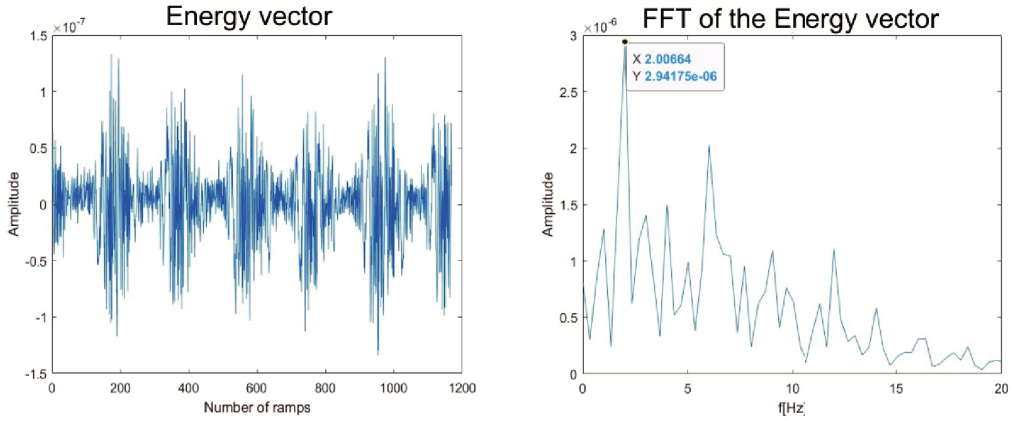

Figure 7. The energy vector from Equation (14) is depicted in the left figure. The right figure shows the frequency spectrum of the left figure.

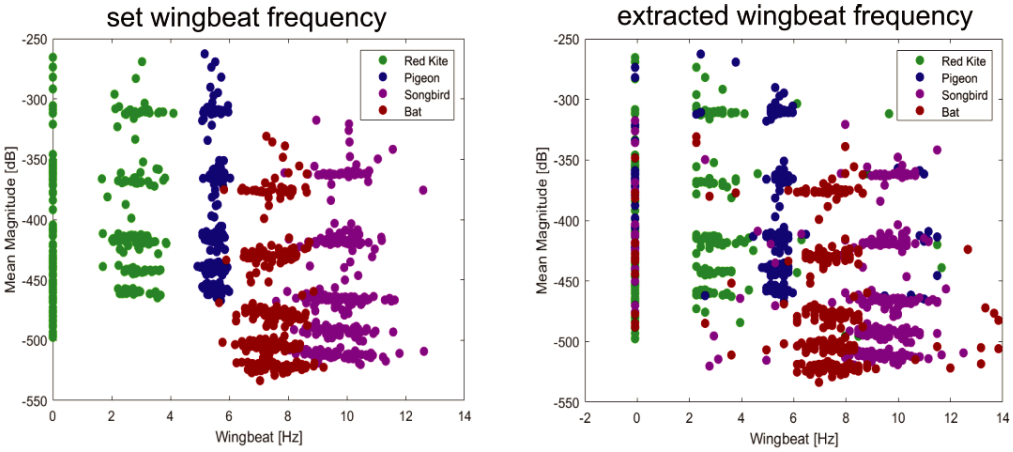

Figure 8. The left figure shows the set wing beat frequency for the simulations against the calculated magnitude. The right figure shows the extracted wing beat frequencies.

calculate the mean:

$$E_i = \frac{1}{n}\sum_{j=1}^{n}|R(i,j)|^2 \tag{14}$$

The transformation of the energy vector E_i into frequency spectrum gives us the wing beat frequency:

$$f_{wingbeat} = \max(FFT(E_i)) \tag{15}$$

The result of Equation (14) is depicted in Figure 7. With this method we are able to extract the wing beat frequencies of flying animals.

As the second classification feature we determine the energy vector and calculated the average power of the energy. It has been found that the average power of the energy vector is a good indication of the size of the birds depending on the distance. In Figure 8 we can see the extracted wing beat frequencies from 1140 simulations and the calculated magnitude. Here we can see the variations in magnitude caused by different distances. As can be seen in the figure, the set frequencies for the birds and bat could be extracted very well. Since the amplitude is dependent on the measured distance, the distance was assumed to be the third feature in the classification (Figure 9).

After testing both SVM and Decision Tree, it turned out that the predictions of the Decision Tree have a significantly better accuracy than those of the the SVM for this classification problem.

Table 1. The confusion matrix of the classification algorithm, which describes the performance of a classifier.

	Bat	**Pigeon**	**Red Kite**	**Songbird**
Bat	71	0	2	5
Pigeon	1	69	12	0
Red Kite	1	2	67	2
Songbird	3	0	0	50

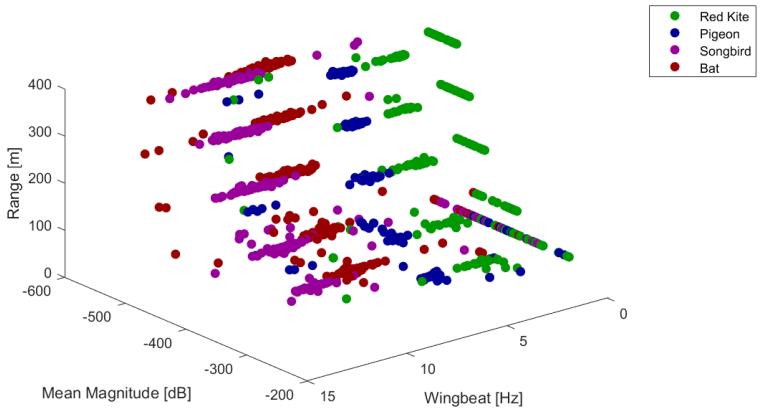

Figure 9. This figure shows the features for the classification which consists of the extracted wing beat frequencies, the calculated magnitude and the detected range.

Therefore, for further analysis, we used the Decision Trees as the basis for classification. With this classification model, we were able to achieve 90.18% accuracy. Table 1 presents the confusion matrix of the classification.

Since the simulation data was simulated for discrete distances from the radar, regardless of the classification result, we wanted to run simulations with randomly chosen distances to validate the classification algorithm. Therefore, we performed 5 simulations with randomly chosen flying animals at the following distances: 74 m, 232 m, 112 m, 267 m, 319 m. The classification algorithm was able to classify correctly in all these 5 cases.

4. CONCLUSION

In this work a simulation environment was developed, with which it is possible to simulate different flying animals activity scenarios at the WT. The goal of this work was the development of localization and classification algorithms that allow us to detect, localize, and classify different flying animals by radar. This allowed us to model three different bird species and one bat species and classify them with 90.18% accuracy. By modeling different bird and bat species, further feature extraction methods could be developed in the future, which could lead to more accurate classification algorithms. The application of these algorithms on WTs could lead to a timely detection of flying animals and their flight behavior, which can be very crucial for the development of an adaptive WT control.

ACKNOWLEDGMENT

The authors gratefully acknowledge the partial financial support of this research by the Federal Ministry for Economic Affairs and Energy (Grant Number: 0324323C).

REFERENCES

1. Brinkmann, R., O. Behr, I. Niermann, and M. Reich (eds.), *Entwicklung von Methoden zur Untersuchung und Reduktion des Kollisionsrisikos von Fledermäusen an Onshore-Windenergieanlagen: Ergebnisse eines Forschungsvorhabens*, Umwelt und Raum, Schriftenreihe Institut für Umweltplanung, Cuvillier-Verl., Göttingen, 2011.
2. Saidur, R., N. A. Rahim, M. R. Islam, and K. H. Solangi, "Environmental impact of wind energy," *Renewable and Sustainable Energy Reviews*, Vol. 15, No. 5, 2423–2430, June 2011.
3. Rydell, J., H. Engström, A. Hedenström, J. K. Larsen, J. Pettersson, and M. Green, *The Effect of Wind Power on Birds and Bats — A Synthesis*, 6511, Swedish Environmental Protection Agency, 2012.
4. Grünkorn, T., J. Blew, T. Coppack, O. Krüger, G. Nehls, A. Potiek, M. Reichenbach, J. von Rönn, H. Timmermann, and S. Weitekamp, *Ermittlung Der Kollisionsraten von (Greif)Vögeln Und Schaffung Planungsbezogener Grundlagen Für Die Prognose Und Bewertung Des Kollisionsrisikos Durch Windenergieanlagen (PROGRESS). Schlussbericht Zum Durch Das Bundesministerium Für Wirtschaft Und Energie (BMWi) Im Rahmen Des 6. Energieforschungsprogrammes Der Bundesregierung Geförderten Verbundvorhaben PROGRESS, FKZ 0325300A-D*, 2016.
5. Bulling, L., D. Sudhaus, D. Schnittker, E. Schuster, J. Biehl, and F. Tucci, *Vermeidungsmamaßnahmen Bei Der Planung Und Genehmigung von Windenergieanlagen — Bundesweiter Katalog von Maßnahmen Zur Verhinderung Des Eintritts von Artenschutzrechtlichen Verbotstatbeständen Nach § 44 BNatSchG*, Fachagentur Windenergie an Land, 2015.
6. Mao, X., J. K. Chow, P. S. Tan, K.-F. Liu, J. Wu, Z. Su, Y. H. Cheong, G. L. Ooi, C. C. Pang, and Y.-H. Wang, "Domain randomization-enhanced deep learning models for bird detection," *Scientific Reports*, Vol. 11, No. 1, 639, December 2021.
7. Niemi, J. and J. T. Tanttu, "Deep learning-based automatic bird identification system for offshore wind farms," *Wind Energy*, Vol. 23, No. 6, 1394–1407, 2020.
8. McClure, C. J. W., B. W. Rolek, L. Dunn, J. D. McCabe, L. Martinson, and T. Katzner, "Eagle fatalities are reduced by automated curtailment of wind turbines," *Journal of Applied Ecology*, Vol. 58, No. 3, 446–452, 2021.
9. Linder, A. C., H. Lyhne, B. Laubek, D. Bruhn, and C. Pertoldi, "Quantifying raptors' flight behavior to assess collision risk and avoidance behavior to wind turbines," *Preprints*, 2021, doi: 10.20944/preprints202102.0391.v1.
10. Rahman, S. and D. A. Robertson, "Classification of drones and birds using convolutional neural networks applied to radar micro-doppler spectrogram images," *IET Radar, Sonar and Navigation*, Vol. 14, No. 5, 653–661, 2020.
11. Björklund, S. and N. Wadströmer, "Target detection and classification of small drones by deep learning on radar micro-doppler," *2019 International Radar Conference (RADAR)*, 1–6, 2019.
12. Li, D., R. Chen, J. Gong, and J. Yan, "Comparison of radar signatures based on flight morphology for large birds and small birds," *IET Radar, Sonar and Navigation*, Vol. 14, No. 4, 1365–1369, September 2020.
13. Zaugg, S., G. Saporta, E. van Loon, H. Schmaljohann, and F. Liechti, "Automatic identification of bird targets with radar via patterns produced by wing apping," *Journal of The Royal Society Interface*, Vol. 5, No. 26, 1041–1053, September 2008.
14. Zadeh, A. T., M. Mälzer, D. H. Nguyen, J. Moll, and V. Krozer, "Radar-based detection of birds at wind turbines: Numerical analysis for optimum coverage," *2021 15th European Conference on Antennas and Propagation (EuCAP)*, 1–5, 2021.
15. Nguyen, D. H., J. Ala-Laurinaho, J. Moll, V. Krozer, and G. Zimmer, "Improved sidelobe suppression microstrip patch antenna array by uniform feeding networks," *IEEE Transactions on Antennas and Propagation*, 1–1, 2020.
16. Lipa, B. J. and D. E. Barrick, "FMCW signal processing," 1990.
17. Balanis, C. A., *Advanced Engineering Electromagnetics*, 2nd Edition, John Wiley & Sons Inc., 2012.

18. Cumming, I. G. and F. H. Wong, *Digital Processing of Synthetic Aperture Radar Data: Algorithm and Implementation*, Artech House Publishers, 2005.
19. Lacomme, P., J.-P. Hardange, J.-C. Marchais, and E. Normant, "Noise and spurious signals," *Air and Spaceborne Radar Systems*, 47–58, 2001.
20. Crecraft, D. I. and S. Gergely, *Analog Electronics*, 2002.
21. Scherr, S., R. Afroz, S. Ayhan, S. Thomas, T. Jaeschke, S. Marahrens, A. Bhutani, M. Pauli, N. Pohl, and T. Zwick, "Influence of radar targets on the accuracy of fmcw radar distance measurements," *IEEE Transactions on Microwave Theory and Techniques*, Vol. 65, No. 10, 3640–3647, 2017.
22. Dakin, B. G. R., "The biophysics of bird ight: Functional relationships integrate aerodynamics, morphology, kinematics, muscles, and sensors," *Canadian Journal of Zoology*, Vol. 93, No. 12, 964, 2015.
23. Rahman, S. and D. A. Robertson, "In-flight rcs measurements of drones and birds at k-band and w-band," *IET Radar, Sonar & Navigation*, Vol. 13, No. 2, 300–309, 2019.
24. Urmy, S. S. and J. D. Warren, "Quantitative ornithology with a commercial marine radar: Standard-target calibration, target detection and tracking, and measurement of echoes from individuals and ocks," *Methods in Ecology and Evolution*, Vol. 8, No. 7, 860–869, November 2016.
25. Jahangir, M., B. I. Ahmad, and C. J. Baker, "Robust drone classification using two-stage decision trees and results from sesar safir trials," *2020 IEEE International Radar Conference (RADAR)*, 636–641, 2020.
26. Bruderer, B., D. Peter, A. Boldt, and F. Liechti, "Wing-beat characteristics of birds recorded with tracking radar and cine camera," *Ibis*, Vol. 152, No. 2, 272–291, April 2010.
27. Taylor, L. A., G. K. Taylor, B. Lambert, J. A. Walker, D. Biro, and S. J. Portugal, "Birds invest wingbeats to keep a steady head and reap the ultimate benefits of ying together," *PLOS Biology*, Vol. 17, No. 6, e3000299, June 2019.
28. Mirkovic, D., P. M. Stepanian, J. F. Kelly, and P. B. Chilson, "Electromagnetic model reliably predicts radar scattering characteristics of airborne organisms," *Scientific Reports*, Vol. 6, No. 1, 35637, December 2016.
29. Bruderer, B. and A. G. Popa-Lisseanu, "Radar data on wing-beat frequencies and ight speeds of two bat species," *Acta Chiropterologica*, Vol. 7, No. 1, 73–82, June 2005.
30. Ostertagová, E., "Modelling using polynomial regression," *Procedia Engineering*, Vol. 48, 500–506, Modelling of Mechanical and Mechatronics Systems, 2012.